Applied Catalysis B: Environmental 129 (2013) 566–574

Contents lists available at SciVerse ScienceDirect

Applied Catalysis B: Environmental

journal homepage: www.elsevier.com/locate/apcatb

Comparison of the photocatalytic efficiencies of bare and doped rutile and anatase TiO_2 photocatalysts under visible light for phenol degradation and *E. coli* inactivation

G. Veréb[a], L. Manczinger[b], G. Bozsó[c], A. Sienkiewicz[d], L. Forró[d], K. Mogyorósi[a,*], K. Hernádi[a], A. Dombi[a]

[a] Research Group of Environmental Chemistry, Institute of Chemistry, Faculty of Sciences and Informatics, University of Szeged, H-6720, Szeged, Tisza Lajos krt. 103, Hungary
[b] Department of Microbiology, Faculty of Sciences and Informatics, University of Szeged, H-6701, P.O. Box 533, Szeged, Hungary
[c] Department of Mineralogy, Geochemistry, and Petrology, Faculty of Sciences and Informatics, University of Szeged, H-6701, P.O. Box 651, Szeged, Hungary
[d] FSB, IPMC, LPMC, Station 3, Ecole Polytechnique Fédérale de Lausanne, CH-1015 Lausanne, Switzerland

ARTICLE INFO

Article history:
Received 15 June 2012
Received in revised form
22 September 2012
Accepted 26 September 2012
Available online 8 October 2012

Keywords:
Photocatalysis
Visible light
Disinfection
Hydroxyl radical
Doped titania
ESR
Singlet oxygen

ABSTRACT

This study aimed at comparing the photocatalytic efficiencies of various TiO_2 based photocatalysts for phenol degradation and bacteria inactivation under illumination with visible light. Commercial undoped anatase and rutile (both from Aldrich), Aeroxide P25 (Evonik Industries), nitrogen-doped anatase (Sumitomo TP-S201, Sumitomo Chemical Inc.), nitrogen and sulphur co-doped anatase (Kronos VLP7000, Kronos Titan GmbH), and our custom-synthesized nitrogen- and iron-doped TiO_2, as well as nitrogen and sulphur co-doped Aeroxide P25 and silver- and gold-deposited Aeroxide P25 were studied. The photocatalytic efficiency of different types of titanium dioxide based photocatalysts was determined by inactivation of *Escherichia coli* K12 bacteria and by phenol decomposition. Electron spin resonance (ESR) in combination with spin trapping was used to get insight into the reactive oxygen species (ROS)-mediated photocatalytic processes in the presence of TiO_2-based photocatalysts. ESR results confirmed that titanias which generated $OH^\bullet$ radicals were efficient in *E. coli* disinfection, whereas titanias that were unable to produce $OH^\bullet$ radicals did not reveal significant bactericidal action. Three of our home-made titanias (iron-, nitrogen-, nitrogen/sulphur) as well as the commercial nitrogen/sulphur codoped Kronos VLP7000 TiO_2 showed higher efficiency of phenol degradation than the well-established reference photocatalyst, Aeroxide P25, but showed much lower (if any) activity for bacteria inactivation, including Kronos VLP7000, which revealed extremely high efficiency for phenol decomposition. Interestingly undoped Aldrich rutile (with large particles - 100–700 nm) had the highest efficiency for inactivation of *E. coli* and also had fairly high activity of phenol degradation.

1. Introduction

Photocatalysis is an intensively investigated alternative water treatment method nowadays which is a promising technique to decompose organic pollutants in water. A very important advantage of photocatalytic purification procedures is that it is applicable for a wide range of organic pollutants. The method is suitable for deactivation of various microorganisms as well. Due to its high efficiency, low toxicity, excellent physico-chemical stability, and low relative costs, titanium dioxide (titania, TiO_2) is considered as the most promising photocatalyst for environmental purification. The first report on TiO_2 based water disinfection was published in 1985 by Matsunaga et al. [1]. Since this work, inactivation studies of many model microorganisms were carried out in the presence of TiO_2-based photocatalysts.

In the majority of these studies, UV irradiation was applied to purify water and inactivate microorganisms in the presence of various forms of titania [1–14]. However it is well known that in the solar spectrum there is a much higher intensity in the visible light range (~43% of total solar energy) than in the UV range (~3%) [8,15], and in an environmentally friendly and economical process, solar irradiation could be applied to activate the photocatalyst [16–21]. Therefore it is important to develop visible light active photocatalysts which are able to decompose organic pollutants and to kill bacteria. Visible light active photocatalysts are also important for indoor applications, *e.g.* in air and surface purification at which naturally UV light is practically absent. In particular, visible light activated detoxification and/or disinfection processes have been reported for TiO_2 doped with nitrogen [13,22–25], iron [26–28], iodine [8,29–33], sulphur [13,22,34], as well as for metal-modified TiO_2, *e.g.* with silver [8,23,35] or gold [36].

* Corresponding author. Tel.: +36 62 544 334; fax: +36 62 420 505.
E-mail address: k.mogyorosi@chem.u-szeged.hu (K. Mogyorósi).

0926-3373/$ – see front matter © 2012 Elsevier B.V. All rights reserved.
http://dx.doi.org/10.1016/j.apcatb.2012.09.045

The main goal of this study was to give an overall picture of the performance of different type of bare and modified titanias using visible light for the decomposition of organic pollutants and killing bacteria. The efficiency of several bare, doped (N, Fe, S) and noble metal deposited (Ag, Au) titanium dioxides were compared by phenol degradation and by deactivation of *Escherichia coli*.

We also aimed to investigate the correlation between the efficiency of organic pollution degradation and disinfection performance, as well as to get an insight into the underpinning photocatalytical mechanisms. It is well known that excitation of TiO_2 by photons with energies greater than the band gap yields formation of electron–hole (e^-_{cb})/(h^+_{vb}) pairs, which can either recombine or take part in redox reactions. As a result, different types of reactive oxygen species (ROS) can be formed that are capable of degrading organic pollutants or damaging bacterial cells [2,8,24]. Ireland et al. [2] emphasized the importance of $OH^\bullet$ radicals because in contrast with other type of water treatment technologies (*e.g.*: ozonation, direct photolysis of hydrogen peroxide, and radiolysis) which inherently produce $OH^\bullet$ radical in very small quantities ($<10^{-12}$ M) [37], in a photocatalytic system 10^{-9} M $OH^\bullet$ concentration was measured [38]. Authors published that there was no inactivation of *E. coli* in the presence of the $OH^\bullet$ radical scavenger [2]. Many other authors recognized the importance of $OH^\bullet$ generation in photocatalytic disinfection processes [2,3,5,6,8,24,34,39–43]. Kikuchi et al. [40] published that the photocatalytic bactericidal effect of *E. coli* on illuminated TiO_2 was confirmed on both oxidation and reduction sites, corresponding to $OH^\bullet$ and $O_2^{\bullet-}$ production, respectively. However the actual lethal agent is H_2O_2, subsequently produced from $OH^\bullet$ and $O_2^{\bullet-}$, particularly in the long-range bactericidal effect [40]. In addition Rengifo-Herrera et al. [13] reported that superoxide radical ($O_2^{\bullet-}$) and its oxidation product: $^1O_2$ – singlet oxygen were responsible for *E. coli* inactivation by N, S co-doped TiO_2 nanoparticles under visible light illumination. In this study, we used electron spin resonance (ESR) spectroscopy to explore the possible differences in efficiencies and the generated ROS by selected doped and undoped titania-based photocatalysts.

2. Experimental

2.1. Commercial photocatalysts

Aeroxide P25 (TiO_2-P25, *Evonik Industries*), Aldrich anatase (TiO_2-AA), and Aldrich rutile (TiO_2-AR) were selected as commercially available undoped photocatalysts.

TiO_2-TP-S201 (Sumitomo Chemical Inc.) and TiO_2-VLP700 (Kronos Titan GmbH) doped with nitrogen and nitrogen/sulphur, respectively, were chosen as commercially available doped TiO_2 based photocatalysts.

2.2. Home made TiO_2 based photocatalysts

The home-made titanias were nitrogen (TiO_2-N), iron (TiO_2-Fe), sulphur and nitrogen (TiO_2-P25-NS) doped and silver (TiO_2-P25-Ag) and gold (TiO_2-P25-Au) deposited titanium dioxide photocatalysts.

Nitrogen doped titania (TiO_2-N) was prepared by the hydrolysis of titanium(IV) chloride in nitric acid solution followed by the addition of aqueous solution of ammonia. The precipitate was then dried and calcinated in our newly developed calcination process using rapid heating (∼60 °C/min) and short exposure to the hot environment at 400 °C for 10 min [25].

Iron doped sample (TiO_2-Fe) was prepared by the oxidative hydrolysis of titanium(III) chloride in the presence of iron(III) chloride under air [27,44]. This sample was also calcinated applying rapid heating and short exposure to the hot environment (at 600 °C for 10 min).

Silver and gold nanoparticles were photodeposited under UV irradiation from silver acetate and $HAuCl_4$ solutions on Aeroxide P25 to produce TiO_2-P25-Ag and TiO_2-P25-Au photocatalysts [44,45]. These two samples contained 1 wt% of the noble metals.

Aeroxide P25 was also co-doped with sulphur and nitrogen by calcination with thiourea for 1 h, at 400 °C in static air (TiO_2-P25-NS) similarly like in the method applied by Rengifo-Herrera et al. [22].

All of the titanias (including the commercial titanium dioxides) were washed three times by centrifugation in 0.1 mM NaCl (Spektrum 3D, 99.0%) aqueous solution, resuspended in MilliQ water, then dried at 80 °C for 24 h and reground in agate mortar before the photocatalytic experiments.

2.3. Methods and instrumentation

2.3.1. XRD

A Rigaku diffractometer was applied for X-ray diffraction (XRD) measurements (λCu Kα = 0.15406 nm, 30 kV, and 15 mA, in the 20–40° (2Θ) regime). The average diameters of the particles were derived using the Scherrer equation. The weight fraction of anatase and rutile was calculated from the peak areas of the anatase and rutile peaks at 25.3° (2Θ) and 27.5° (2Θ), respectively.

2.3.2. DRS

The DR spectra of the samples (λ = 220–800 nm) were measured by a JASCO-V650 diode array computer controlled (SpectraManager Software) spectrophotometer with an integration sphere (ILV-724).

2.3.3. TEM

TEM micrographs were recorded on a Philips CM 10 instrument operating at 100 kV using Formvar coated copper grids.

2.3.4. BET

The specific surface area of the catalysts was determined by nitrogen adsorption at 77 K using a Micromeritics gas adsorption analyser (Gemini Type 2375). The specific surface area was calculated using the BET method.

2.3.5. X-ray photoelectron spectroscopy (XPS)

X-ray photoelectron spectra were taken with a SPECS instrument equipped with a PHOIBOS 150 MCD 9 hemispherical electron energy analyser operated in the FAT mode. Further details of the measurements are described elsewhere [46].

2.3.6. X-ray fluorescence spectroscopy (XRF)

A Horiba Jobin Yvon XGT-5000 X-ray fluorescent spectrometer, equipped with Rh X-ray source was used to measure the element content of the samples. The records were made at 30 kV excitation voltage, 0.5 mA anode current and 1000 s measuring time.

2.3.7. ESR spin trapping measurements

The ESR measurements were performed at room temperature by using a Bruker ESP300E spectrometer (Bruker BioSpin, Germany), operating at the X-band frequency and equipped with a standard rectangular TE_{102} cavity. After each illumination step, small aliquots of ∼20 μL were transferred into 0.7 mm ID and 0.87 mm OD glass capillary tubes (VitroCom, NJ, USA). To maximize the sample volume in the active zone of the ESR cavity, assemblies of seven tightly packed capillaries were bundled together and inserted into a wide-bore quartz capillary (standard ESR quartz tube with 2.9 mm ID and 4 mm OD, Model 707-SQ-250 M, from Wilmad-LabGlass Inc., Vineland, NJ, USA). Such setup resulted in *ca.* 140 μL sample volume in the active zone of the TE_{102} cavity,

Fig. 1. Photograph of used photoreactor system equipped with conventional 24 W energy saving compact fluorescence lamps.

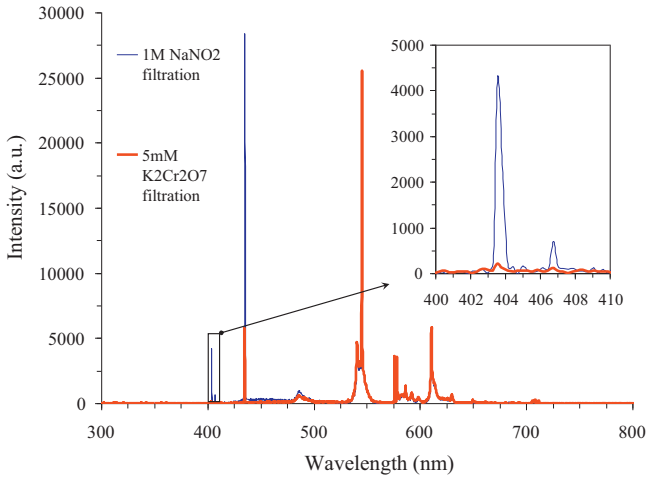

Fig. 2. Spectra of the applied conventional energy saving compact fluorescence lamps (24 W) with 1 M $NaNO_2$ and 5 mM $K_2Cr_2O_7$ light cut-off filtrations by the recirculation of these solutions in the thermostating jacket.

which, together with the division of the aqueous sample into seven physically-separated volumes, markedly improved the overall sensitivity of measurements [47,48]. The typical instrumental settings were: microwave frequency 9.77 GHz, microwave power 10.1 mW, sweep width 100 G, modulation frequency 100 kHz, modulation amplitude 0.5 G, receiver gain 2×10^4, time constant 81.92 ms, conversion time 40.96 ms and total scan time 41.9 s.

2.4. Measurements of photocatalytic activity

2.4.1. Experimental conditions for phenol degradation

The experiments of phenol (Spektrum 3D, 99.0%) degradation were carried out in a special photoreactor which was an open glass vessel with double walls, surrounded by a thermostating jacket at 25.0 °C. Around the reactor four compact fluorescence lamps (DÜWI 25920/R7S-24W type – conventional 24 W energy saving compact fluorescence lamps) were mounted (Fig. 1). The spectrum of the lamp was slightly modified by circulating 1 M $NaNO_2$ (Molar Chemicals, min. 99.13%) aqueous solution in the thermostating jacket. This cut-off solution absorbs UV photons below 400 nm, providing visible light irradiation for the samples (Fig. 2). The radiation intensity was determined by ferrioxalate actinometry for the VIS lamps with $NaNO_2$ cut-off filter solution as $I_{VIS,1} = 1.07 \pm 0.03 \times 10^{-5}$ einstein/dm^3/s in the photoreactor. (It should be noted that the average quantum yield of ferrioxalate actinometry is about 0.9 in the wavelength range between 400 and 540 nm, and it is nearly zero above 540 nm [49].)

The efficiency of different type of photocatalysts was determined by decomposing phenol (0.1 mM) in NaCl solution (0.9 wt%) which contained the titania powders in 1.0 g/L concentration. The suspension (100 mL) was sonicated before the photocatalytic tests (for 5 min) then it was stirred by magnetic stirrer and air was bubbled during the experiments. Changes in phenol concentration were followed using an Agilent 1100 series HPLC system equipped with Lichrospher RP 18 column applying methanol/water mixture as eluent (the detection was carried out at 210 nm).

2.4.2. Experimental conditions for inactivation of E. coli

The same photoreactor and similar conditions were applied like for the phenol decomposition measurements. Another type of light filtration was also carried out in some experiments. Applying 5 mM $K_2Cr_2O_7$ (Reanal, analytical grade) aqueous solution in the thermostating jacket, the light intensity was reduced to 4% below 420 nm Fig. 2. The radiation intensity was determined by ferrioxalate actinometry for the VIS lamps with the $K_2Cr_2O_7$ cut-off filter solution as $I_{VIS,2} = 1.75 \pm 0.01 \times 10^{-6}$ einstein/dm^3/s in the photoreactor.

The *E. coli* suspensions were prepared using the following procedure. Firstly, *E. coli* cultures were grown for 24 h in 0.9% NaCl solution supplemented with nutrients: 1% Tripton (Reanal, analytical grade) and 0.5% yeast extract (Scharlau, analytical grade). Then the cultures were washed two times with a 0.9% saline solution by centrifugation at 4000 rpm for 2 min and the sediment was re-suspended in 0.9% NaCl solution. Prior to the disinfection experiments, the TiO_2-based photocatalysts were added to a 0.9% NaCl solutions and sonicated to form homogeneous suspensions, which were then supplemented with the previously prepared *E. coli* suspensions.

A low value of initial colony forming unit (10^4 CFU/mL) was set in the titanium dioxide suspensions in order to determine very low disinfection efficiencies as well. Samples were plated on agar gels during the experiments and the colonies were counted after 24 h of incubation at 37 °C in dark. All of the samples were plated on 2–3 agar gels for getting reliable data. All of the presented results were taken from the average of two parallel experiments (results were fairly reproducible).

2.4.3. Experimental conditions for ESR measurements

In the ESR measurements we used two (ROS) scavengers, *i.e.* 10 mM concentration of 2,2,6,6-tetramethyl-4-piperidinol (TMP-OH) and 50 mM concentration of 5,5-dimethyl-1-pyrroline N-oxide (DMPO). The solutions of ROS scavengers were prepared either in H_2O or deuterated water (D_2O). TMP-OH, and D_2O (isotopic purity of 99.9 at% D) were purchased from Sigma–Aldrich (Switzerland) and used as received. DMPO was also obtained from Sigma–Aldrich (Switzerland). Before the ESR measurements the suspensions were sonicated for 5 min and then, during the subsequent photocatalytic experiments under exposure to visible light, they were vigorously stirred by magnetic stirrer and air was bubbled through. The aqueous suspensions containing the titanium dioxide nanoparticles and ROS scavengers were exposed to the visible light in the same photoreactor in which phenol decomposition and disinfection experiments were carried out. Similarly, the same conventional (24 W) energy saving compact fluorescence lamps and 1 M $NaNO_2$ solution in the thermostating jacket for light cut-off filtration were

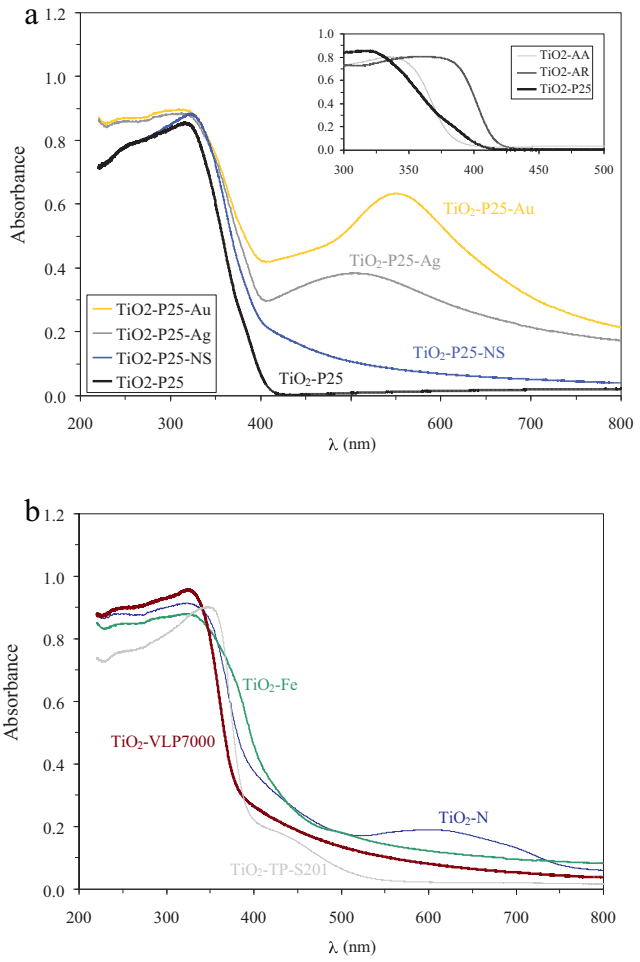

Fig. 3. Diffuse reflectance spectra of investigated photocatalysts: (a) non-doped commercial and P25 based modified home-made titanium dioxides; (b) doped commercial and home-made titanias.

used. The concentration of the titanium dioxide suspensions was of 1.0 g/L, and the total volume was of 20 mL.

3. Results and discussion

3.1. Characterization of the photocatalysts

The photocatalysts were characterized by several methods, including: XRD, transmission electron microscopy (TEM), X-ray fluorescence spectroscopy (XRF), diffuse reflectance spectroscopy (DRS), X-ray photoelectron spectroscopy (XPS) and nitrogen gas adsorption analysis (BET) method. The most important physico-chemical parameters of the studied photocatalysts, *i.e.* anatase and rutile content, the particle size, the dopant content (derived from XRF, and/or XPS) as well as the BET specific surface area, are shown in Table 1. There are investigated titanias which contain only anatase phase (such as TiO_2-AA and TiO_2-VLP7000), in the P25 based titanias more than 90% of the particles are in anatase phase, in the nitrogen doped titania 5% brookite content was determined by XRD, while Aldrich rutile contains 96% rutile. The particle sizes are very different: TiO_2-VLP7000 has the smallest particles (D_{XRD} = 7.8 nm) with the largest specific surface area (297 m^2/g), while Aldrich rutile contains large particles (100–700 nm), which results in very low specific surface area (2.7 m^2/g). The light absorption was measured by diffuse reflectance spectroscopy for all of the photocatalysts (Fig. 3a and b). These figures show that doped

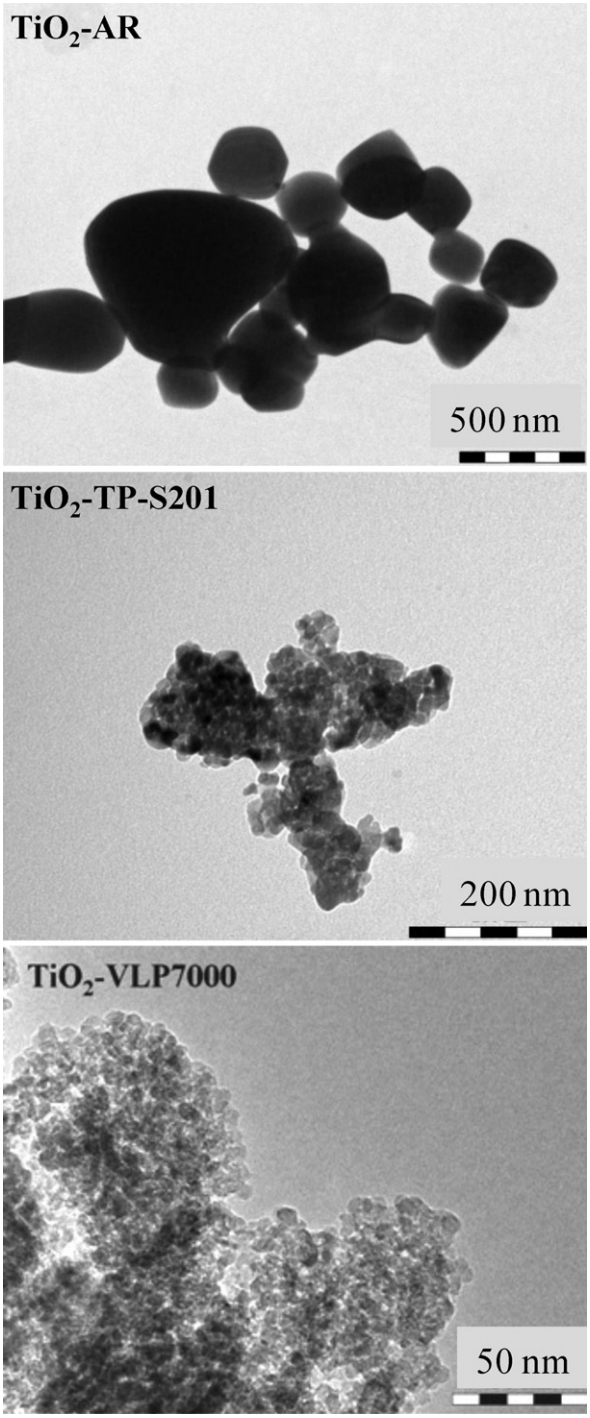

Fig. 4. TEM images of (a) Aldrich rutile, (b) Sumitomo TP-S201 and (c) Kronos VLP7000 titanias. TEM images of other investigated photocatalysts are published elsewhere [44].

titanias absorb visible light. Aldrich anatase does not absorb any photons beyond 400 nm, however Aldrich rutile has a band gap at about 420 nm. These titanias were all examined with transmission electron microscopy to observe the size distribution and the morphology of the particles. The TEM images of TiO_2-TP-S201, TiO_2-VLP7000 and TiO_2-AR are illustrated in Fig. 4, while other images of the photocatalysts are published elsewhere [44]. Aldrich rutile sample contains relatively large particles which are larger than 100 nm ($D_{TEM} \approx 315$ nm) which results in very low specific surface area. The particle diameter values calculated from the line

Table 1
Structural parameters of the investigated photocatalysts (phase content, particle size, the concentration of dopants and specific surface area), the initial degradation rates of phenol, irradiation time for total sterilization and the results of ESR measurements are shown. The samples are listed in the order of decreasing activity for phenol degradation form the top to the bottom. Grey rows indicate the home-made titanium dioxides, the white rows are for commercial titanias.

Sample	Anatase (wt%)	Rutile (wt%)	D_A (nm)	D_R (nm)	Dopant content (at%)[f]	a^S_{BET} (m^2/g)	$r_{0,phenol}$ ($\times 10^{-8}$ M/s)	$t_{sterilization}$ (min)[g]	ESR Measurements		
									With TMP-OH scavenger $^1O_2$	With DMPO scavenger $O_2^{\bullet-}$	With DMPO scavenger $OH^{\bullet}$
TiO_2-VLP7000	100	–	7.8	–	S:0.33[c]/N:1.21[d]	297	29.9	–	High	No	No
TiO_2-AR	4	96		~315[b]	–	2.7	4.2	20	No	No	High
TiO_2-P25-NS	94	6	25.4	~40	S:0.13[c]/N: n.d.	55	3.7	–		Not measured	
TiO_2-N	95[a]	–	6.5	–	1.32[d]	139	2.4	–	No	No	No
TiO_2-Fe	29	71	~35	~31	0.37[c]	28	1.7	–		Not measured	
TiO_2-TP-S201	100	–	17.3	–	N:0.82[d]	80	1.5	60		Not measured	
TiO_2-P25	90	10	25.4	~40	–	49	1.4	60	No	No	Yes
TiO_2-P25-Ag	90	10	24.5	~42	0.24[c,e]	51	1.3	60		Not measured	
TiO_2-P25-Au	90	10	24.1	~37	0.13[c,e]	51	0.4	–		Not measured	
TiO_2-AA	100	–	>85	–	–	9.9	0.4	–		Not measured	

[a] Calculated content of brookite is 5 wt%, D_B = 14.4 nm.
[b] Average particle diameter was calculated from TEM pictures.
[c] Measured by XRF.
[d] Estimated by XPS.
[e] Nominal (added) metal content is 1.0 wt% as $m_D/m_{catalyst} \times 100$; measured values for Ag and Au contents are 0.94 wt% and 0.96 wt%, respectively.
[f] Expressed as $n_D/n_{total} \times 100$.
[g] CFU = 10^4; 1 M $NaNO_2$ light cut-off filtration ($\lambda > 400$ nm).

broadening of the anatase peak for TiO_2-TP-S201 (D_{XRD} = 17.3 nm) and TiO_2-VLP7000 (D_{XRD} = 7.8 nm) samples are in good agreement with the nanoparticle sizes observed on their TEM images (Table 1, Fig. 4b and c).

3.2. Phenol degradation

The decomposition of phenol was followed by HPLC. The decay curves are presented in Fig. 5a and b. There was not any decrease in the concentration under irradiation without photocatalyst, and only very slow degradations were observed applying Aldrich anatase or TiO_2-P25-Au. It means that in the later case depositing Au nanoparticles on titanium dioxide reduces the phenol degradation efficiency in the visible light range. The TiO_2-TP-S201 and the TiO_2-P25-Ag samples showed similar performance than the well known reference Aeroxide P25 (TiO_2-P25), which decomposed 17% of the phenol from the 0.1 mM solution after 4 h of irradiation. Three home-made titanias showed higher efficiency than TiO_2-P25. Only commercially available Kronos VLP7000 (co-doped by nitrogen and sulphur) had better performance than the non-doped Aldrich rutile (TiO_2-AR). It should be noted that rutile absorbs light between 400 and 420 nm (in contrast with the anatase), in which wavelength range there are two peaks in the spectrum of the lamp (Fig. 2). Nevertheless, the most active photocatalyst (TiO_2-VLP7000) contains 100% anatase phase. The high performance of this titania was resulted by the efficient doping providing the ability to activate the particles by visible light. The decay curves, and also the initial degradation rates of phenol demonstrate as well, that TiO_2-VLP7000 has extremely high efficiency for phenol degradation, 94% of phenol was decomposed in 4 h. KRONOS VLP7000 is a nitrogen and sulphur co-doped titanium dioxide like our home-made TiO_2-N,S, but the commercial titania owns very high specific surface area which can result in this high performance besides the efficient doping (Kim and Choi [50] published that high specific surface area is beneficial for the degradation of phenol).

3.3. Disinfection performance

Investigating Aldrich anatase, TiO_2-P25-Au, TiO_2-Fe, TiO_2-N; TiO_2-P25-NS and TiO_2-VLP7000 titanium dioxides, there was not any disinfection effect observed after 2 h of irradiation. The results

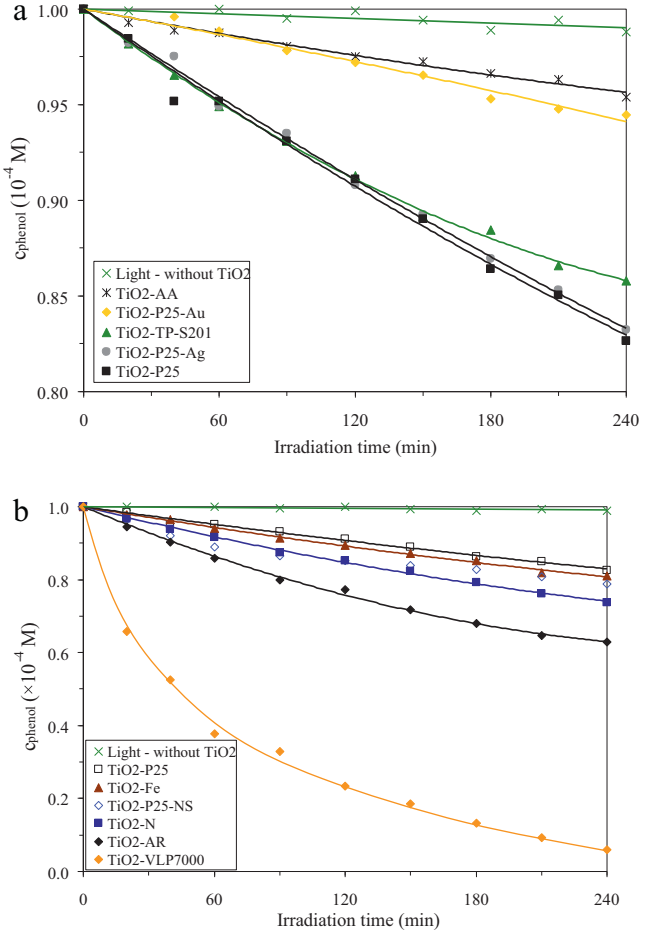

Fig. 5. (a and b) Decay curves of phenol under VIS irradiation (conventional 24 W energy saving compact fluorescence lamps with 1 M $NaNO_2$ light cut-off filtration ($\lambda > 400$ nm).

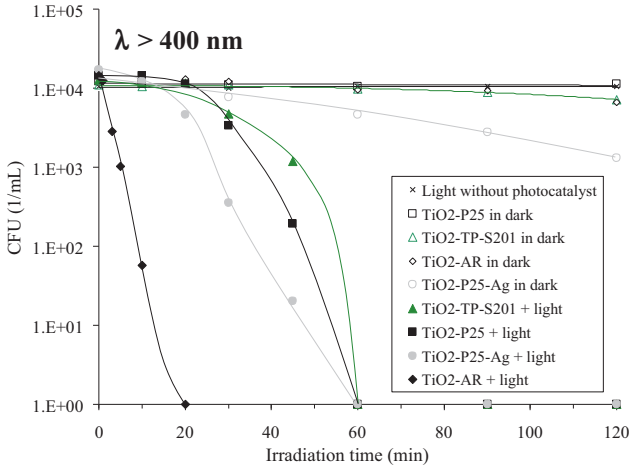

Fig. 6. Disinfection experiments with 1 M $NaNO_2$ filtered visible light irradiation (initial colony forming unit was 10^4).

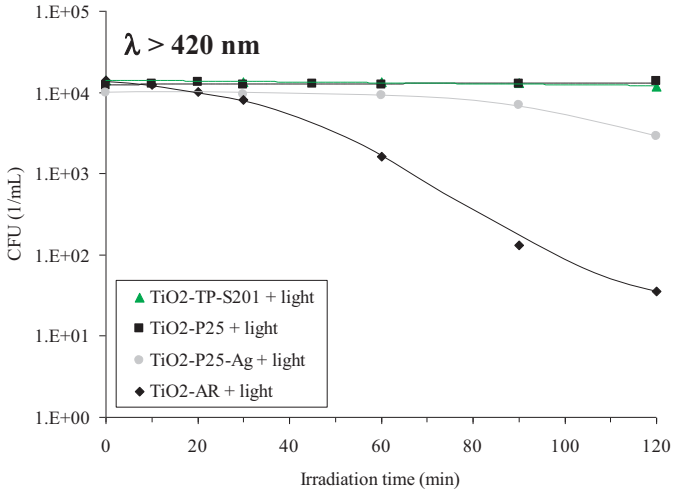

Fig. 7. Disinfection experiments with 5 mM $K_2Cr_2O_7$ filtered visible light irradiation (initial colony forming unit was 10^4).

of the five other photocatalysts activities are presented in Fig. 6. All of the experiments were repeated two times, and the averages are showed. Applying TiO_2-TP-S201, TiO_2-P25 and TiO_2-P25-Ag titanias, the colony forming unit was reduced to zero in 1 h. From the shape of the mortality curve, it seems that the silver containing sample has a little bit higher disinfection ability than the silver free P25. It is most likely due to the well known disinfection effect of silver ions [51–57] which can be released from the silver nanoparticles to the solution in low quantity (in the dark experiment a slow disinfection effect was also determined on this photocatalyst). TiO_2-AR sample had much higher activity for inactivation of *E. coli*. The water was sterilized totally by this titania in 20 min (Fig. 6).

A series of experiments was also carried out to exclude the possibility that the determined disinfection effects were resulted by toxic compounds dissolved from the irradiated photocatalysts. Suspensions of the titanias (without bacteria addition) were irradiated for the same time at which they disinfected previously the solution, and then the nanoparticles were separated by centrifugation and filtration. After the separation, 10^4 CFU/mL was adjusted to this solution, and it was poured back into the photoreactor and the changes in colony forming unit was followed for 2 h of irradiation. In the case of TiO_2-P25, TiO_2-TP-S201, TiO_2-AR titanias, there was not seen any notable CFU reduction. Only in the case of silver containing TiO_2 was noticed a similar CFU reduction like in TiO_2-Ag suspension in dark.

Investigation of disinfection performance was carried out also at higher initial CFU (10^5 CFU/mL) for the most active titania (TiO_2-AR). This titania totally sterilized the water after 30 min of irradiation in this case.

Disinfection experiments were also carried out with another type of light cut-off filtration. Applying 5 mM $K_2Cr_2O_7$ aqueous solution in the thermostating jacket the light intensity was reduced to 4% below 420 nm (Fig. 2). Results of disinfection experiments are presented in Fig. 7. Fig. 8 represents a photograph which demonstrates the *E. coli* colonies of the photocatalytic test with Aldrich rutile (after 24 h of thermostating in 37 °C, in dark). Applying Aeroxide P25 or TiO_2-TP-S201 there was not seen any disinfection effect after 2 h. The silver containing TiO_2 sample showed a low activity for killing bacteria like in dark condition (due to the presence of Ag^+ ions). Non-doped Aldrich rutile showed a notable activity considering the very low light intensity below 420 nm (only light $\lambda < 420$ nm can excite this phase of titanium dioxide). With $K_2Cr_2O_7$ filtration three titanium dioxides (TiO_2-P25, TiO_2-P25-Ag, TiO_2-TP-S201) lost their photocatalytic disinfection property, however with $NaNO_2$ cut-off filtration, these titanias disinfected completely the water in 1 h. This means that the intensity of the commercially available light sources in the wavelength range from 400 nm to 420 nm is crucial for efficient indoor air/surface cleaning.

3.4. Comparison of phenol degradation and the disinfection performance

The results of phenol decomposition and disinfection experiments are summarized in Table 1. The values of initial degradation rates of phenol for the different titanias are decreasing from the top to the bottom. TiO_2-VLP7000 showed extremely high efficiency for phenol decomposition, but it had not any notable disinfection property. Aldrich rutile had high efficiency to kill bacteria and also had high efficiency for phenol degradation. There were three titanias which degraded phenol with high efficiency but did not show any antibacterial property. Moreover, there were three other titanias which killed *E. coli* after 1 h of irradiation, however these titanium dioxides had relatively low performance for phenol degradation. It seems from Table 1, there is no correlation between the bacteria killing ability of catalyst and their crystalline structure. Interpretation for these interesting observations based on the particle size or on the specific surface area cannot be provided. To get some

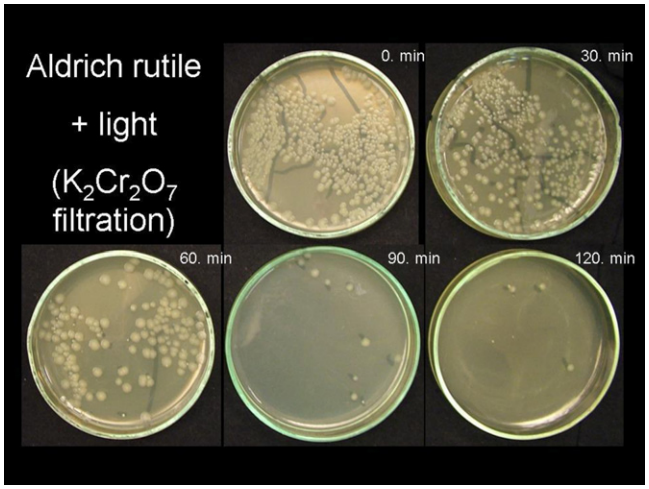

Fig. 8. Photograph of *E. coli* colonies of the photocatalytic test ($\lambda > 420$ nm initial CFU = 10^5) with Aldrich rutile (after 24 h thermostating in 37 °C, in dark).

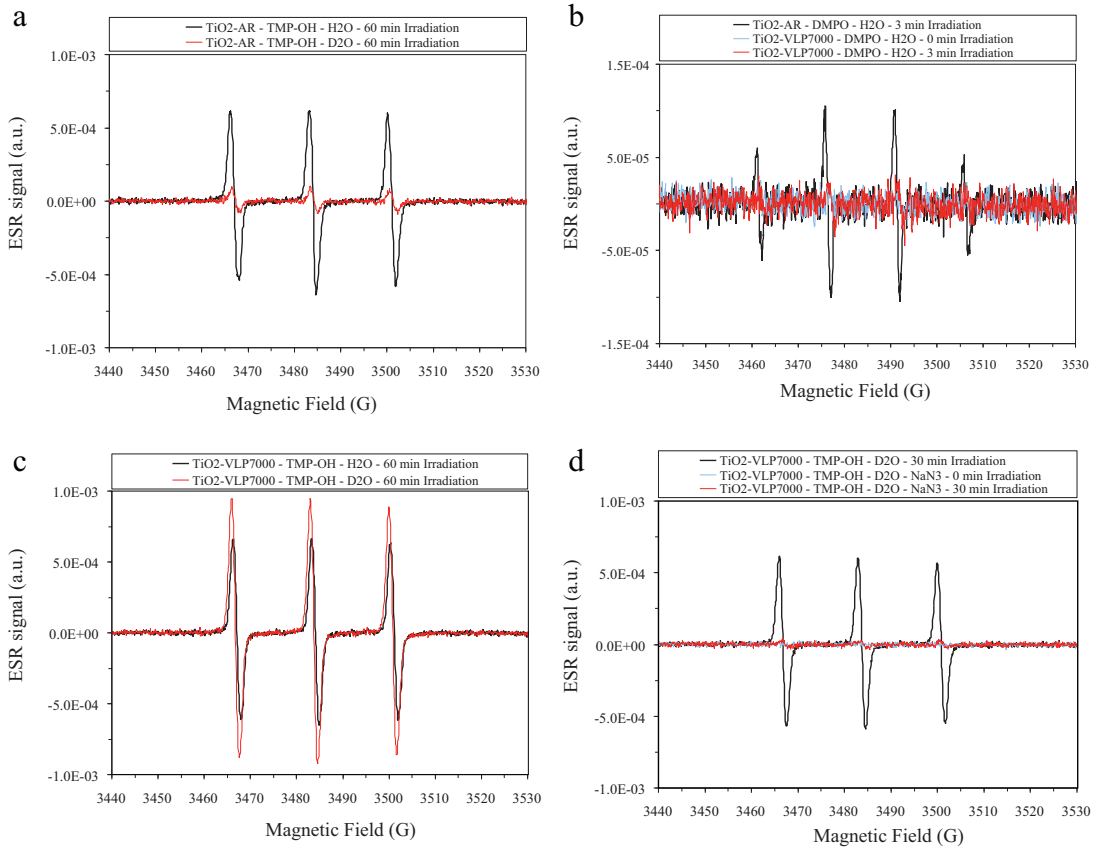

Fig. 9. Results of ESR measurements: (a) visible light illuminated aqueous (H_2O and D_2O) suspensions of TiO_2-AR containing 10 mM concentration of TMP-OH; (b) visible light illuminated aqueous suspensions of TiO_2-AR and TiO_2-VLP7000 containing 50 mM concentration of DMPO; (c) visible light illuminated aqueous (H_2O and D_2O) TiO_2-VLP7000 suspensions containing 10 mM concentration of TMP-OH; (d) visible light illuminated D_2O suspension of TiO_2-VLP7000 containing 10 mM TMP-OH (in the presence and absence of NaN_3 singlet oxygen quencher).

insight into ROS-mediated bacteria inactivation mechanisms, ESR spin-trapping measurements were carried out for selected photocatalysts.

3.4.1. ESR measurements

Four selected titanium dioxides were investigated. TiO_2-VLP7000 and TiO_2-N showed rapid phenol degradation, but no *E. coli* deactivation. TiO_2-AR had high efficiency for phenol degradation and for disinfection as well, while TiO_2-P25 had antibacterial property but it had relatively low performance for phenol degradation. The results of the ESR measurements are summarized in Table 1.

3.4.1.1. TiO_2-AR. In the presence of TMP-OH scavenger in the VIS irradiated TiO_2-AR suspension a strong ESR signal of TEMPOL was observed after 1 h of illumination (Fig. 9a). TEMPOL might be produced by an attack of singlet oxygen ($^1O_2$) or hydroxyl radical ($OH^\bullet$) on TMP-OH [58].

The ESR signal of TEMPOL is slightly distorted. As it is seen in Fig. 9a the central ESR feature is markedly higher than the low- and high-field features. This distortion originates from the formation of another nitroxide radical, TEMPONE. $OH^\bullet$ radicals can react with TEMPOL by attacking on the OH-groups which yield the generation of TEMPONE [59].

In D_2O, as it can be seen in Fig. 9a, the signal amplitude of the ESR signal of TEMPOL was reduced *ca.* 7.3 times as compared to H_2O (for the same illumination time). It is known that D_2O suppresses the formation of $OD^\bullet$ radicals at the TiO_2/D_2O interface [60,61].

In the presence of DMPO an intense DMPO-$OH^\bullet$ signal (in H_2O) was observed under visible light irradiation which proved the $OH^\bullet$ radical generation in the case of AR (Fig. 9b). This result corroborates with the marked diminishment of the TEMPOL signal in D_2O, and suggests that the photocatalytic activity of this sample might be related to the photocatalytic generation of hydroxyl radicals ($OH^\bullet$).

It should be noted that TiO_2-AR probably produces some $^1O_2$ *via* the classical mechanism suggested by Nosaka et al. [62] but since applying DMPO scavenger no DMPO-OOH signal was detected, TiO_2-AR do not produce $O_2^{\bullet-}$ radical in measurable quantity.

3.4.1.2. TiO_2-VLP7000. Under VIS light illumination in H_2O, the TiO_2-VLP7000 sample gave a strong TEMPOL signal. This signal is even stronger (by *ca.* 10%) than the signal of the TiO_2-AR (Fig. 9c).

In D_2O, the ESR signal amplitude of TEMPOL increased *ca.* 1.4 times as compared to H_2O (Fig. 9c) which suggested that the detected signal can be due to the generation of singlet oxygen ($^1O_2$) on the surface of TiO_2-VLP7000. To get more evidence of the generation of $^1O_2$ an experiment with singlet oxygen quencher was also carried out. In D_2O a very strong suppression of the TEMPOL signal was observed (it was reduced *ca.* 19 times) in the presence of 100 mM NaN_3 (which is a $^1O_2$ quencher) (see Fig. 9d).

So both the ESR signal enhancement in D_2O and signal quenching by NaN_3 suggested that the strong signal of TEMPOL is due to the formation of $^1O_2$. However these results do not exclude the possibility that the scavenger was directly oxidized on the surface of the photocatalyst, as suggested by Nosaka (in 2006) for other titania photocatalysts [63], considering that this titania has extremely high specific surface area.

In the presence of DMPO scavenger no DMPO-OH or DMPO-OOH signal was determined for VIS light irradiated TiO_2-VLP7000 (Fig. 9b) which proved that there is no OH• radical generation on this titania. This observation corroborates with the results of the experiments with TMP-OH scavenger.

3.4.1.3. TiO_2-P25. At the case of TMP-OH scavenger in the visible light illuminated TiO_2-P25 suspension a well measurable signal of TEMPOL was observed, which was about 30% of the signal of TiO_2-AR. This signal was strongly decreased in D_2O like in the case of TiO_2-AR, and the experiments with DMPO scavenger also proved again the generation of OH• radical (but in smaller amounts than in the case of TiO_2-AR) and the absence of $O_2^{\bullet -}$.

3.4.1.4. TiO_2-N. No marked formation of OH•, $O_2^{\bullet -}$ or singlet oxygen ($^1O_2$) was observed for the nitrogen doped home-made titania (TiO_2-N).

4. Conclusions

Under visible light illumination, three of our home-made titanias (TiO_2-Fe, TiO_2-N,S, TiO_2-N,) and commercial nitrogen/sulphur-doped Kronos VLP7000 titanium dioxide showed higher efficiency for phenol degradation than the well known reference Aeroxide P25, however only VLP7000 had better performance than non-doped Aldrich rutile.

Aldrich rutile had high efficiency of *E. coli* inactivation and also had significant activity for phenol degradation; however four doped titanias had higher efficiency for phenol degradation than TiO_2-P25 but had not any activity for inactivation of bacteria.

ESR measurements pointed out that titanias that generated OH• radicals were active for killing *E. coli*, and those, which were unable to produce OH• radicals did not show any disinfection property. This is consistent with the statements of many authors who described that OH• radicals play a major role in photocatalytic disinfection experiments [2,5,6,24,34,39,42,43], and recent study proved that this persist in the case of visible light irradiation as well. This is in good agreement with the results of the study of Yu et al. [34] who demonstrated the deactivation of *Micrococcus lylae* by visible light irradiated TiO_2 due to the generation of hydroxyl radical.

Kronos VLP7000 showed extremely high efficiency for phenol decomposition due to its high specific surface area, but this titania did not show any disinfection property under our circumstances which might be due to absence of OH• radical generation.

TiO_2-N titania showed high performance for phenol decomposition, however neither OH• radical nor superoxide radical ion ($O_2^{\bullet -}$) or singlet oxygen ($^1O_2$) was detected. This means that phenol degradation occurred *via* the reaction by the hole on the surface, and the high efficiency is most likely due to the high specific surface area (this titanium dioxide has the second highest specific surface area among the investigated samples).

The experiments with $K_2Cr_2O_7$ cut-off filtered light source pointed out that the rutile could have high-performance applicability for utilizing visible light in self-cleaning or disinfecting processes. Rutile had a notable efficiency also with this very low intensity below 420 nm. This study firstly investigated the disinfection performance of rutile particles with relatively large particle size ($d \sim 315$ nm) using solely visible light for activating the photocatalyst.

Pure and silver doped P25 and Sumitomo titania sterilized water in 1 h when $\lambda > 400$ nm condition was used, but these photocatalysts lost their disinfection property when $K_2Cr_2O_7$ light cut-off filtration was applied ($\lambda > 420$ nm). These results highlighted that the intensity of the commercially available lamps in the wavelength range from 400 nm to 420 nm is crucial to apply effectively the photocatalysts for indoor air/surface cleaning.

Acknowledgements

This work was partially financed by the European Union through the Hungary-Serbia IPA Cross-border Co-operation Program, HU-SRB/0901/121/116. It was also co-financed by the grant from the Hungarian National Office of Research and Technology (OTKA CK 80193), by the European Regional Development Fund (TÁMOP-4.2.1/B-09/1/KONV-2010-0005 and TÁMOP-4.2.2/B-10/1-2010-0012) and the Swiss Contribution (SH/7/2/20).

KM thanks the financial support of the Hungarian Research Foundation (OTKA PD78378) and the János Bolyai Research Scholarship of the Hungarian Academy of Sciences.

A.S and L.F. acknowledge the financial support of the Swiss National Science Foundation through the Nano-Tera NTF project "Core-shell superparamagnetic and upconverting nano-engineered materials for biomedical applications – NanoUp".

The authors are indebted to Evonik Industries, to Kronos Gmbh., to Sumitomo Chemicals Inc. for supporting our work by supplying free TiO_2 samples for these studies.

References

[1] T. Matsunaga, R. Tomoda, T. Nakajima, H. Wake, FEMS Microbiology Letters 29 (1985) 211–214.
[2] J.C. Ireland, P. Klostermann, E.W. Rive, R.M. Clark, Applied and Environmental Microbiology 59 (1993) 1668–1670.
[3] J.A. Herrera-Melian, J.M.D. Rodriguez, A.V. Suarez, E.T. Rendon, C.V.D. Campo, J. Arana, J.P. Pena, Chemosphere 41 (2000) 323–327.
[4] K. Kühn, Chemosphere 53 (2003) 71–77.
[5] M. Cho, H. Chung, W. Choi, J. Yoon, Water Research 38 (2004) 1069–1077.
[6] A. Vohra, D.Y. Goswami, D.A. Deshpande, S.S. Block, Applied Catalysis B 64 (2006) 57–65.
[7] A.K. Benabbou, Z. Derriche, C. Felix, P. Lejeune, C. Guillard, Applied Catalysis B 76 (2007) 257–263.
[8] C. Hu, J. Guo, J. Qu, X. Hu, Langmuir 23 (2007) 4982–4987.
[9] C. Guillard, T. Bui, C. Felix, V. Moules, B. Lina, P. Lejeune, Comptes Rendus Chimie 11 (2008) 107–113.
[10] D.M.A. Alrousan, P.S.M. Dunlop, T.A. McMurray, J.A. Byrne, Water Research 43 (2009) 47–54.
[11] L. Caballero, K.A. Whitehead, N.S. Allen, J. Verran, Journal of Photochemistry and Photobiology A: Chemistry 202 (2009) 92–98.
[12] F. Chen, X. Yang, Q. Wu, Environmental Science & Technology 43 (2009) 4606–4611.
[13] J.A. Rengifo-Herrera, K. Pierzchała, A. Sienkiewicz, L. Forró, J. Kiwi, C. Pulgarin, Applied Catalysis B 88 (2009) 398–406.
[14] E.A. Kozlova, A.S. Safatov, S.A. Kiselev, V.Y. Marchenko, A.A. Sergeev, M.O. Skarnovich, E.K. Emelyanova, M.A. Smetannikova, G.A. Buryak, A.V. Vorontsov, Environmental Science & Technology 44 (2010) 5121–5126.
[15] S. Malato, P. Fernández-Ibáñez, M.I. Maldonado, J. Blanco, W. Gernjak, Catalysis Today 147 (2009) 1–59.
[16] A. Vidal, A.I. Dıaz, A.E. Hraiki, M. Romero, I. Muguruza, F. Senhaji, J. González, Catalysis Today 54 (1999) 283–290.
[17] E. Duffy, Solar Energy 77 (2004) 649–655.
[18] C. Sichel, J. Blanco, S. Malato, P. Fernández-Ibáñez, Journal of Photochemistry and Photobiology A: Chemistry 189 (2007) 239–246.
[19] C. Sichel, J. Tello, M. de Cara, P. Fernández-Ibáñez, Catalysis Today 129 (2007) 152–160.
[20] A.I. Gomes, J.C. Santos, V.J.P. Vilar, R.A.R. Boaventura, Applied Catalysis B 88 (2009) 283–291.
[21] C. Karunakaran, G. Abiramasundari, P. Gomathisankar, G. Manikandan, V. Anandi, Journal of Colloid and Interface Science 352 (2010) 68–74.
[22] J.A. Rengifo-Herrera, J. Kiwi, C. Pulgarin, Journal of Photochemistry and Photobiology A: Chemistry 205 (2009) 109–115.
[23] P. Wu, J.A. Imlay, J.K. Shang, Biomaterials 31 (2010) 7526–7533.
[24] P. Wu, R. Xie, J.A. Imlay, J.K. Shang, Applied Catalysis B 88 (2009) 576–581.
[25] Z. Pap, L. Baia, K. Mogyorosi, A. Dombi, A. Oszko, V. Danciu, Catalysis Communications 17 (2011) 1–7.
[26] K. Nagaveni, G. Sivalingam, M.S. Hegde, G. Madras, Environmental Science & Technology 38 (2004) 1600–1604.
[27] Z. Ambrus, N. Balazs, T. Alapi, G. Wittmann, P. Sipos, A. Dombi, K. Mogyorosi, Applied Catalysis B 81 (2008) 27–37.
[28] E.G. Bajnoczi, N. Balazs, K. Mogyorosi, D.F. Sranko, Z. Pap, Z. Ambrus, S.E. Canton, K. Noren, E. Kuzmann, A. Vertes, Z. Homonnay, A. Oszko, I. Palinko, P. Sipos, Applied Catalysis B 103 (2011) 232–239.

[29] X. Hong, Z. Wang, W. Cai, F. Lu, J. Zhang, Y. Yang, N. Ma, Y. Liu, Chemistry of Materials 17 (2005) 1548–1552.
[30] G. Liu, Z. Chen, C. Dong, Y. Zhao, F. Li, G.Q. Lu, H.M. Cheng, Journal of Physical Chemistry B 110 (2006) 20823–20828.
[31] S. Song, J.J. Tu, Z.Q. He, F.Y. Hong, W.P. Liu, J.M. Chen, Applied Catalysis A 378 (2010) 169–174.
[32] Z.Q. He, C. Wang, H.Y. Wang, F.Y. Hong, X.H. Xu, J.M. Chen, S. Song, Journal of Hazardous Materials 189 (2011) 595–602.
[33] Z.Q. He, L.Y. Zhan, F.Y. Hong, S. Song, Z.Y. Lin, J.M. Chen, M.T. Jin, Journal of Environmental Sciences – China 23 (2011) 166–170.
[34] J.C. Yu, W. Ko, J. Yu, H. Yip, P.K. Wong, J. Zhao, Environmental Science & Technology 39 (2005) 1175–1179.
[35] R.G. Nair, J.K. Roy, S.K. Samdarshi, A.K. Mukherjee, Colloids and Surfaces B: Biointerfaces 86 (2011) 7–13.
[36] M.V. Dozzi, L. Prati, P. Canton, E. Selli, Physical Chemisty Chemical Physics 11 (2009) 7171–7180.
[37] W.R. Haag, J. Hoigné, Chemosphere 14 (1985) 1659–1671.
[38] J.C. Ireland, J. Valinieks, Chemosphere 25 (1992) 383–396.
[39] D. Gumy, A. Rincon, R. Hajdu, C. Pulgarin, Solar Energy 80 (2006) 1376–1381.
[40] Y. Kikuchi, K. Sunada, T. Iyoda, K. Hashimoto, A. Fujishima, Journal of Photochemistry and Photobiology A: Chemistry 106 (1997) 51–56.
[41] P.S.M. Dunlop, J.A. Byrne, N. Manga, B.R. Eggins, Journal of Photochemistry and Photobiology A: Chemistry 148 (2002) 355–363.
[42] S. Malato, J. Blanco, D.C. Alarcón, M.I. Maldonado, P. Fernández-Ibáñez, W. Gernjak, Catalysis Today 122 (2007) 137–149.
[43] O.K. Dalrymple, E. Stefanakos, M.A. Trotz, D.Y. Goswami, Applied Catalysis B 98 (2010) 27–38.
[44] G. Veréb, Z. Ambrus, Z. Pap, Á. Kmetykó, A. Dombi, V. Danciu, A. Cheesman, K. Mogyorósi, Applied Catalysis A: General 417–418 (2012) 26–36.
[45] K. Mogyorosi, A. Kmetyko, N. Czirbus, G. Vereb, P. Sipos, A. Dombi, Reaction Kinetics and Catalysis Letters 98 (2009) 215–225.
[46] Z. Pap, V. Danciu, Z. Cegléd, Á. Kukovecz, A. Oszkó, A. Dombi, K. Mogyorósi, Applied Catalysis B 101 (2011) 461–470.
[47] Y.E. Nesmelov, D.D. Thomas, Journal of Magnetic Resonance 178 (2006) 318–324.
[48] J.I. Nieto-Juarez, K. Pierzchla, A. Sienkiewicz, T. Kohn, Environmental Science & Technology 44 (2010) 3351–3356.
[49] Taylor & Francis Group, LLC, Handbook of Photochemistry, third ed., 2006.
[50] S. Kim, W. Choi, Journal of Physical Chemistry B 109 (2005) 5143–5149.
[51] R.B. Thurman, C.P. Gerba, Critical Reviews in Environmental Control 18 (1988) 295–315.
[52] A.M. Pisarevskii, A.V. Kaverin, G.P. Lepnev, Y.I. Nikolaev, Russian Journal of Applied Chemistry +71 (1998) 1482–1484.
[53] C.W. Beer, L.E. Guilmartin, T.F. McLoughlin, T.J. White, Journal of Environmental Health 61 (1999) 9–12.
[54] L. Hitchcock, J.R. Anderson, D. Johnson, T.J. White, Journal of Environmental Health 62 (2000) 27–31.
[55] R.A. Khaydaroy, R.R. Khaydarov, R.L. Olsen, S.E. Rogers, Journal of Water Supply Research and Technology-Aqua 53 (2004) 567–572.
[56] D.S. Blanc, P. Carrara, G. Zanetti, P. Francoli, Journal of Hospital Infection 60 (2005) 69–72.
[57] B. Van Aken, L.S. Lin, Water Science and Technology 64 (2011) 1226–1232.
[58] I. Rosenthal, C.M. Krishna, G.C. Yang, T. Kondo, P. Riesz, FEBS Letters 222 (1987) 75–78.
[59] K. Saito, K. Takeshita, J.I. Ueda, T. Ozawa, Journal of Pharmaceutical Sciences 92 (2003) 275–280.
[60] J. Cunningham, S. Srijaranai, Journal of Photochemistry and Photobiology A: Chemistry 43 (1988) 329–335.
[61] P.K.J. Robertson, L.A. Lawton, B. Cornish, M. Jaspars, Journal of Photochemistry and Photobiology A: Chemistry 116 (1998) 215–219.
[62] Y. Nosaka, T. Daimon, A.Y. Nosaka, Y. Murakami, Physical Chemisty Chemical Physics 6 (2004) 2917–2918.
[63] Y. Nosaka, H. Natsui, M. Sasagawa, A.Y. Nosaka, Journal of Physical Chemistry B 110 (2006) 12993–12999.